



NRL/MR/6791--16-9703

# Millimeter Wave Radar for Atmospheric Turbulence Characterization and Wind Profiling for Improved Naval Operations

BENJAMIN ROCK  
BAHMAN HAFIZI  
RICHARD FISCHER

*Beam Physics Branch  
Plasma Physics Division*

ANTONIO TING

*Research Support Instruments  
Lanham, Maryland*

December 29, 2016

Approved for public release; distribution is unlimited.

<b>REPORT DOCUMENTATION PAGE</b>				<b>Form Approved OMB No. 0704-0188</b>	
Public reporting burden for this collection of information is estimated to average 1 hour per response, including the time for reviewing instructions, searching existing data sources, gathering and maintaining the data needed, and completing and reviewing this collection of information. Send comments regarding this burden estimate or any other aspect of this collection of information, including suggestions for reducing this burden to Department of Defense, Washington Headquarters Services, Directorate for Information Operations and Reports (0704-0188), 1215 Jefferson Davis Highway, Suite 1204, Arlington, VA 22202-4302. Respondents should be aware that notwithstanding any other provision of law, no person shall be subject to any penalty for failing to comply with a collection of information if it does not display a currently valid OMB control number. <i>PLEASE DO NOT RETURN YOUR FORM TO THE ABOVE ADDRESS.</i>					
<b>1. REPORT DATE (DD-MM-YYYY)</b> 29-12-2016		<b>2. REPORT TYPE</b> Interim		<b>3. DATES COVERED (From - To)</b> April 2016 – December 2016	
<b>4. TITLE AND SUBTITLE</b>  Millimeter Wave Radar for Atmospheric Turbulence Characterization and Wind Profiling for Improved Naval Operations				<b>5a. CONTRACT NUMBER</b>	
				<b>5b. GRANT NUMBER</b>	
				<b>5c. PROGRAM ELEMENT NUMBER</b>	
<b>6. AUTHOR(S)</b>  Benjamin Rock, Bahman Hafizi, Richard Fischer, and Antonio Ting*				<b>5d. PROJECT NUMBER</b> 67-1E43-07	
				<b>5e. TASK NUMBER</b>	
				<b>5f. WORK UNIT NUMBER</b>	
<b>7. PERFORMING ORGANIZATION NAME(S) AND ADDRESS(ES)</b>  Naval Research Laboratory 4555 Overlook Avenue, SW Washington, DC 20375-5320				<b>8. PERFORMING ORGANIZATION REPORT NUMBER</b>  NRL/MR/6791--16-9703	
<b>9. SPONSORING / MONITORING AGENCY NAME(S) AND ADDRESS(ES)</b>  Naval Research Laboratory 4555 Overlook Avenue, SW Washington, DC 20375-5320				<b>10. SPONSOR / MONITOR'S ACRONYM(S)</b>  NRL 6.1	
				<b>11. SPONSOR / MONITOR'S REPORT NUMBER(S)</b>	
<b>12. DISTRIBUTION / AVAILABILITY STATEMENT</b>  Approved for public release; distribution is unlimited.					
<b>13. SUPPLEMENTARY NOTES</b>  *Research Support Instruments, 4325 Forbes Blvd., Lanham, MD 20706.					
<b>14. ABSTRACT</b>  In this report, we consider the capabilities of a millimeter-wave radar to make atmospheric air flow measurements relevant to naval operations. The measurements could provide data that may be used to generate a map of the turbulent air flow fields in the vicinity of aircraft and aircraft carriers and to characterize the prevailing atmospheric turbulence. One application of these types of measurements is for improved safety of carrier based takeoff and landing. For both fixed wing aircraft and rotorcraft, takeoff and landing are two of the most hazardous operations. Data from measurements of the complex airflows surrounding ships can be used to determine operational envelopes, more efficiently space incoming aircraft, and can be used in conjunction with simulations to inform and influence ship design. Another application is for high-energy laser propagation. Various adaptive optics schemes have been developed in order to compensate for the deleterious effects of atmospheric effects on laser propagation. Accurate knowledge of the level and type of turbulence along the laser path could be used to inform an adaptive optics system.					
<b>15. SUBJECT TERMS</b> Turbulence                      Bragg scattering Doppler weather radar        Rayleigh scattering					
<b>16. SECURITY CLASSIFICATION OF:</b>			<b>17. LIMITATION OF ABSTRACT</b>  Unclassified Unlimited	<b>18. NUMBER OF PAGES</b>  17	<b>19a. NAME OF RESPONSIBLE PERSON</b> Benjamin Rock
<b>a. REPORT</b> Unclassified Unlimited	<b>b. ABSTRACT</b> Unclassified Unlimited	<b>c. THIS PAGE</b> Unclassified Unlimited			<b>19b. TELEPHONE NUMBER (include area code)</b> (202) 767-3708



## **Contents**

<b>I. Introduction and Review of Naval Atmospheric Sensing Needs</b>	<b>2</b>
A. Flow Field Mapping Near Naval Carriers	2
B. High Energy Laser Propagation and Adaptive Optics Systems	4
<b>II. Microwave Interaction with the Atmosphere</b>	<b>5</b>
A. Rayleigh Scattering	5
B. Bragg Scattering	7
C. Comparison of Rayleigh and Bragg Scattering	9
D. Combined Bragg/Rayleigh Scattering	11
<b>III. Air Flow Measurements with Radar</b>	<b>12</b>
<b>IV. Conclusions</b>	<b>14</b>
<b>References</b>	<b>14</b>



# Millimeter Wave Radar for Atmospheric Turbulence Characterization and Wind Profiling for Improved Naval Operations

Ben Rock, Bahman Hafizi and Rich Fischer

*Plasma Physics Division, U.S. Naval Research Laboratory, Washington, DC 20375*

Tony Ting

*Research Support Instruments, Lanham, Md 20706*

## Abstract

In this report, we consider the capabilities of a millimeter-wave radar to make atmospheric air flow measurements relevant to naval operations. The measurements could provide data that may be used to generate a map of the turbulent air flow fields in the vicinity of aircraft and aircraft carriers and to characterize the prevailing atmospheric turbulence. One application of these types of measurements is for improved safety of carrier based takeoff and landing. For both fixed wing aircraft and rotorcraft, takeoff and landing are two of the most hazardous operations. Data from measurements of the complex airflows surrounding ships can be used to determine operational envelopes, more efficiently space incoming aircraft, and can be used in conjunction with simulations to inform and influence ship design. Another application is for high-energy laser propagation. Various adaptive optics schemes have been developed in order to compensate for the deleterious effects of atmospheric effects on laser propagation. Accurate knowledge of the level and type of turbulence along the laser path could be used to inform an adaptive optics system.

## **I. INTRODUCTION AND REVIEW OF NAVAL ATMOSPHERIC SENSING NEEDS**

Atmospheric conditions affect naval operations in a wide variety of ways. From an aviation perspective, both fixed wing aircraft such as F/A-18s and rotorcraft such as V-22s must navigate through powerful environmentally and self generated turbulent airflows as they takeoff and land. Turbulent mixing of multiple airflows generated by different sources can lead to complicated and unpredictable conditions that further endanger already complicated take off and landing operations. From a directed energy weapons (DEW) perspective, refractive index variations generated by atmospheric turbulence along a high energy laser (HEL) beam path can cause excessive beam spreading and breakup of the laser beam. Both of these effects lead to reduced power density on target and lengthened kill time. In this report, we will examine the ability of high resolution radar to perform atmospheric sensing measurements relevant to Naval aviation and DEW/HEL operations. We begin with a discussion of previous efforts to mitigate the aforementioned difficulties, and argue that millimeter wave radar techniques can be used to supplement and/or supplant the existing techniques.

### **A. Flow Field Mapping Near Naval Carriers**

It is well known that the air-flow characteristics over the decks of naval ships, and the interactions with aircraft/rotorcraft lead to restrictions in operability conditions of the craft. Examples are restrictions in operable weather conditions and the need to establish specific wind-over-deck conditions for successful landing (e.g. steering the carrier into the wind). On landing approach, fixed-wing aircraft must navigate through the airwake, often called the “burble” generated by the carrier deck and superstructure. Rotorcraft must operate in the mixed airflow from the turbulence generated by the ship’s superstructure and it’s own rotor generated downwash and turbulent vortices.

The Airwake Analysis team at NAVAIR, led by Susan Polsky, has developed CFD (computational fluid dynamics) models to evaluate and analyze the airflow characteristics behind and around a number of Navy ships, including aircraft carriers and amphibious assault carriers. Airflow parameters are used to determine operational envelopes for aircraft as well

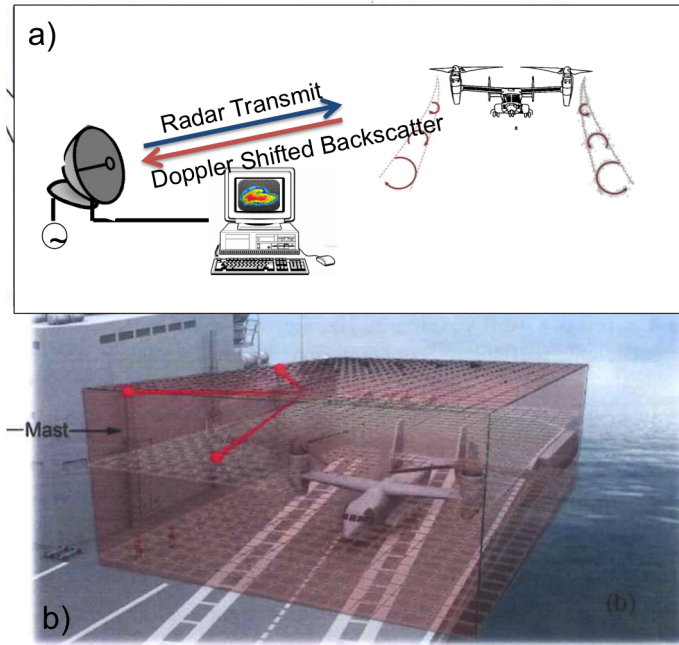


FIG. 1: A multi-static radar system for detection of three-component air velocity fields. (a) A cartoon depiction of radar system measuring turbulent vortices generated by a rotorcraft. (b) A cartoon depiction of a rotorcraft operating near the superstructure of a carrier. An ideal system would be able to determine the air velocity field within a region approximately 400 ft x 160 ft x 40 ft surrounding the rotorcraft with 2ft spatial resolution and at a rate of 20 Hz. Practical systems which could measure airflow within subvolumes of this region at the desired resolution and rate would be also of significant value. (adapted from Reference [1].)

as to inform and influence ship design. There have been two recent SBIR programs funded by the Navy to develop near-infrared lidar systems to profile the airflows near and on naval carriers [1]. The goal was to demonstrate that the technology could be used to provide accurate inflow conditions for the CFD models, to validate and test the model predictions, and possibly be used in real time to inform the pilot and carrier operators to improve aviation safety.

These SBIR efforts ultimately failed for at least two reasons. First, the clear air echoes from lidar were below noise levels in the detectors ( $\text{SNR} < 0 \text{ dB}$ ). Second, the mechanical steering and ranging mechanisms could not operate quickly enough to map a significant volume faster than the airflow in the volume evolved. When the air was seeded with smoke

particles, the SNR improved and radial air velocity measurements could be obtained in a particular resolution volume. However, it is not clear that the spatial resolution would have been adequate, and it is unlikely that the system could ever be made to work in rain or fog. A workaround for the slow scan rate may not be achievable with current lidar technology. The general conclusion of multiple independent efforts was that lidar technology is not sufficiently developed to address this Naval need.

Laser and microwave radiation are both electromagnetic in origin, and hence, the same range equation describes radar and lidar, and many of the same considerations apply to both of them. Because of the similarities, the same configuration that was foreseen for the lidar systems could be employed for a radar system (Fig. 1). Two important places where lidar and radar differ are in scattering cross section and detection. A third difference arises between radar and the attempted airwake lidar systems in how range resolution is approached. Each of these differences, and the methods developed for handling them, presents an opportunity for radar to improve over lidar for air flow-field mapping applications.

## **B. High Energy Laser Propagation and Adaptive Optics Systems**

Effective beam control of high energy lasers (HELs) is a key component of a laser weapon system. Turbulence can have a significant deleterious effect on the propagation of the HEL beam. Propagation of a laser beam in turbulence results in large intensity scintillations on the target and additional beam spreading. The scintillations are caused by induced air index of refraction variations which are approximately determined as  $n = 1 + 77.6 \times 10^{-6}(1 + 0.00752\lambda^{-2})P/T$ , where P is pressure in millibars, T is temperature in K,  $\lambda$  is wavelength in microns. Turbulence is characterized by the Rytov variance  $\sigma_R^2$ . Expressed in terms of the refractive index structure constant,  $C_n^2$ , wavelength  $\lambda$  and propagation range  $L_T$ , the Rytov variance is given by  $\sigma_R^2 = \lambda^{-7/6} L_T^{11/6}$ . The intensity scintillations are characterized by an intensity variance  $\sigma_I^2$  that can be expressed in terms of the Rytov variance:  $\sigma_I^2 \approx \sigma_R^2$  for  $\sigma_R^2 < 0.3$  and  $\sigma_I^2 \approx 1 + (\sigma_R^2)^{-2/5}$  for  $\sigma_R^2 \gg 1$ . In many applications it is important to mitigate intensity scintillation. Often adaptive optics (AO) techniques are employed to correct (or compensate for) the phase distortions induced by turbulence. Adaptive optics techniques typically employ a beacon beam whose sole purpose to interrogate the atmospheric path of the HEL beam, providing the information necessary to un-do the phase distortions on the

latter. The beacon beam is also affected (and scintillated) by the turbulence. To be useful the AO system must measure the atmospheric conditions at a sufficiently rapid rate as given by, for example, the Greenwood frequency  $1/\tau_G$ . Additionally, the time required to form a tight beacon beam must be short compared to  $\tau_G$ , the time scale for atmospheric change. The Greenwood frequency is given by  $1/\tau_G = v_{wind}/r_0$ , where the transverse coherence length (Fried parameter) is  $r_0 = 0.184(\lambda^2/(C_n^2 L_T))^{3/5} = 0.75 * (\lambda L_T)^{1/2} \sigma_R^2 \sigma_R^{-6/5}$  and is the wind velocity. The mean-square, long-term spot radius is then given by

$$\langle R_L^2(z) \rangle \approx \frac{w^2}{2} \left(1 + \frac{z}{F}\right)^2 + \frac{4z^2}{k_0^2 r_0^2(z)}, \quad (1)$$

for  $r_0(z) \gg \ell_0$  or  $z = 1/C_n^2 k_0^2 \ell^{5/3}$ , where  $w$  is the initial spot radius and  $F$  is the focal length of the optic. These considerations indicate that knowledge of the atmospheric conditions and, in particular, refractive index structure constant is indispensable to effective utilization HEL propagation.

## II. MICROWAVE INTERACTION WITH THE ATMOSPHERE

Radar return signals arise from electromagnetic scatterers within a resolution volume. For meteorological applications, these scatterers are either particulate or molecular. Particulate scatterers are macroscopic particles, and include dust, pollutants and hydrometeors. The particles that are suspended in the atmosphere (as opposed to falling through it) are called aerosols and are typically assumed to contribute individually to the electromagnetic scattering. For wavelengths of 1 micron and longer, molecular scattering arises as a collective effect of variations of the molecular density. This is usually captured as variations of the refractive index of air with pressure. Meteorological weather observations rely on both types of scattering mechanisms, which will be discussed in turn and then compared.

### A. Rayleigh Scattering

In clear unperturbed air, the reflection of electromagnetic waves is relatively weak and proceeds via the scattering from a uniform distribution of aerosols. In this case, the amplitude and range weighting functions are essentially constant spatial functions over the resolution volume, so that the collective scattering contributions become vanishingly small.

The echo return power is then the sum of return powers for each scatterer individually. In terms of scattering cross-sections,  $\sigma_i$ , of the individual scatterers, the expected echo power/density from scatterers at range  $r$  is

$$dP = \frac{1}{2} I \sigma \quad (2)$$

with

$$\sigma = \sum_i^{N_s} \sigma_i, \quad (3)$$

and

$$I = \frac{P_t G^2 \lambda^2 f^4 |W|^2}{4\pi l^2 r^4}, \quad (4)$$

where  $N_s$  is the number of aerosol scatterers,  $P_t$  is the transmitted radar power,  $G$  is the antenna gain, and  $f$  is the angular power gain pattern.

The echo power returned clearly depends on the number density and types of atmospheric aerosols. There are several models which attempt to describe the size distribution and composition of global atmospheric aerosols. One such model, the Advanced Navy Aerosol Model (ANAM), has been developed to model maritime aerosols found in near surface open-ocean conditions, and has an additional predictive capability [2]. In the ocean environment, the aerosols consist of a mixture of salt water aerosols, water soluble aerosols and dust aerosols in a size distribution similar to that shown in Figure 1. ANAM represents different aerosol sizes and composition as modes. The different aerosol modes will have different scattering cross-sections based on their different sizes and refractive indices. ANAM mode 0 represents dust particles of continental origin, mode 1 represents water-soluble aerosols, whereas modes 2-4 represent various aerosols of marine origin. The physical properties of the aerosols are summarized in Table I for a relative humidity level of 80%, a typical level over the open ocean. Aerosols such as dust are not affected by changes in humidity levels, however, all the other particles will grow and their refractive indices will evolve with increasing relative humidity. For a particular set of atmospheric conditions, the aerosol size distribution function  $F(R) = \sum_{j=0}^4 F_j(R)$ , with  $R$  the aerosol radius, is the sum of the size distributions of the modes. The total aerosol density is the integral of the distribution function over all radii, i.e.  $n_A = \int F(R) dR$ . The size distributions of the modes are shown in Fig. 2 for 80% relative humidity at a height approximately 5 m from the sea surface.

As the wavelength decreases, the scattering behavior from aerosols varies from the Rayleigh regime ( $\lambda \gg R$ ) where the cross section varies as  $R^6/\lambda^4$  to the resonant Mie

TABLE I:  $R_A$  is mean radius, Density is integrated number density. The B1 material is Volz' B1 aerosol material [2].

Mode	Material	$R_A$ [ $\mu\text{m}$ ]	Density [ $\text{cm}^{-3}$ ]
0	Non-hygroscopic Dust	0.03	$2.6 \times 10^3$
1	B1 aerosol+Water	0.03	$6.1 \times 10^3$
2	Sea Salt+Water ("aged" aerosol)	0.24	9.0
3	Sea Salt+water (new aerosol)	2	0.014
4	Sea Salt+water (near-surface)	8	0.014
Total			$9.0 \times 10^3$

Regime ( $\lambda \approx R$ ), and ultimately to a geometric regime ( $\lambda \ll R$ ) where the cross section is equal to the physical cross section independent of wavelength. For millimeter wavelengths and longer, the scattering is strictly within the Rayleigh regime. In this case, the radar reflectivity  $\eta_R$  can be estimated by employing the ANAM size distribution function,  $f(R)$ , and the complex refractive index,  $n$ , for water,

$$\eta_R = \frac{(2\pi)^6}{\lambda^4 \pi} |K_W|^2 \int_R R^6 f(R) dR, \quad (5)$$

where  $K_W = (n^2 - 1)/(n^2 + 1)$ . The value of  $|K_W|^2$  at centimeter and millimeter wavelengths is approximately 0.93 for water. A more accurate estimate for the reflectivity would utilize different refractive index values for the different modes. Doppler radar signals from point scatterers provide information on the mean and variance of the point velocities in the resolution volume.

## B. Bragg Scattering

Radar is also able to sense returns from clear air where there is no precipitation, aerosols, or other point targets. The source of the clear air radar returns is index of refraction variations arising from turbulent mixing in the atmosphere. For a combination of dry air and water vapor, the index of refraction varies as  $n^2 = 1 + C_d P_d/T + C_{w1} P_w/T + C_{w2} P_w/T^2$ , where  $P_d$  and  $P_w$  are the partial pressures of dry air and water vapor,  $T$  is the temperature, and  $C_d$ ,  $C_{w1}$ , and  $C_{w2}$  are constants [3]. In the Fraunhofer limit, the scattered electric field

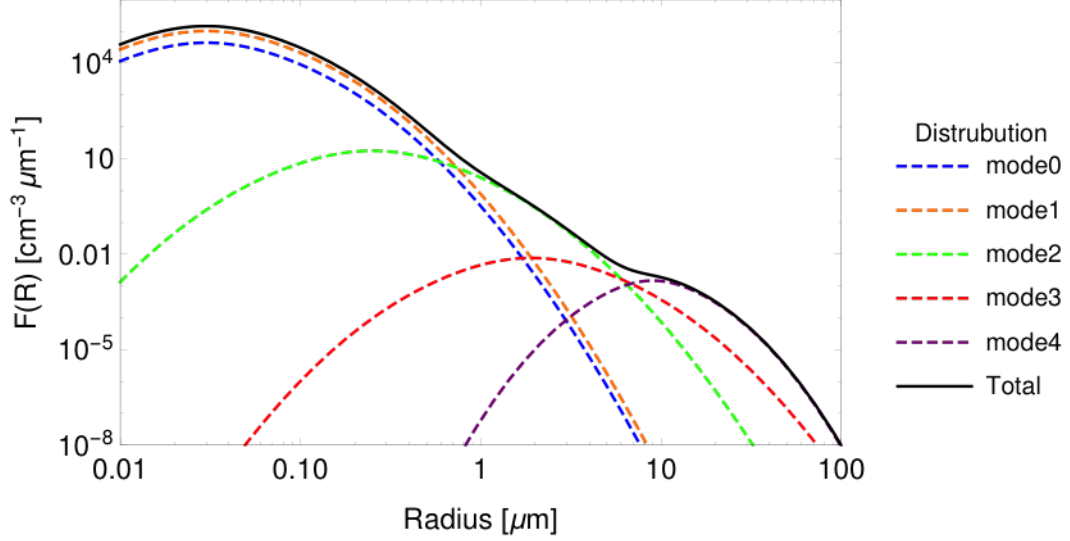


FIG. 2: Naturally occurring aerosol distribution function 5 meters above the ocean surface calculated according to ANAM 3.0 for 80% relative humidity. Dashed curves denote individual aerosol modes 0-4. The solid curve denotes the total aerosol distribution function.

from index of refraction variations is given by

$$\vec{E}_S = \frac{k^2 \vec{a}_r \times (\vec{a}_r \times \vec{A})}{2\pi r^2} \int_V \Delta n(r') e^{-2ikz'} dv', \quad (6)$$

where  $k$  is the wavenumber,  $\vec{A}$  is the incident field amplitude (including polarization), and  $\Delta n$  is the fluctuation of the index of refraction from its average value.

Scattering from index of refraction variations provides an additional radar target in a resolution volume, and in certain circumstances, can also provide finer details of motion (air flow). Turbulent flow at fairly large scales (outer scale length,  $L$ ) cascades down to turbulent flow (eddies) at small scales, down to an inner scale length,  $\ell$ , where viscous dissipation sets in. The cascading of scales in the flow gives rise to space Fourier components in the index of refraction from the outer to the inner scale length (the inertial subrange). From the Fraunhofer scattering equation, the dominant contribution to the back-scattering from a radar at wavelength  $\lambda$  comes from the structure wavelength which satisfies the Bragg condition  $\Lambda = \lambda/2$ . In isotropic, homogeneous turbulence governed by a Kolmogorov-von Karman distribution, the radar reflectivity is given by [4, 5]

$$\eta_B = \frac{\pi^2}{2} k^4 \Phi_n \quad (7)$$

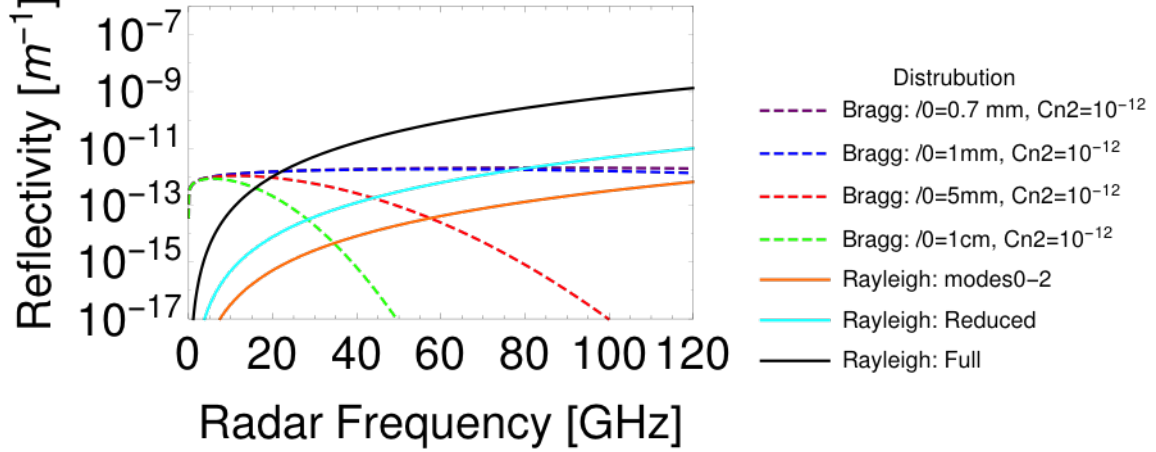


FIG. 3: Radar reflectivity for Rayleigh scattering from hydrometeors and Bragg scattering from isotropic, homogeneous turbulence. The Bragg scattering curves are for  $C_n^2 = 10^{-12}$  and the Rayleigh scattering curves are based on ANAM using the index of refraction for water. The Full Rayleigh distribution uses the total ANAM distribution of Fig. 2. To emphasize the sensitivity to the large aerosol densities, the reduced curve excludes ANAM mode 4 and reduces the mode 3 particle distribution by 10%. The last Rayleigh calculation only includes ANAM modes 0-2.

with,

$$\Phi_n = 0.033C_n^2(k^2 + K_0^2)^{-11/6}e^{-k^2/K_m^2} \quad (8)$$

where  $K_0 = 2\pi/L$ ,  $K_m = 5.92/\ell$  and  $C_n^2$  is the refractive index structure constant defined as

$$C_n^2 = \frac{\langle (n(\vec{r}) - n(\vec{r}'))^2 \rangle}{|\vec{r} - \vec{r}'|}. \quad (9)$$

$\Phi_n$  is the spectral density function defined as the Fourier transform of the refractive index correlation function. The inner scale length over land is typically a few millimeters in the daytime, whereas it may be somewhat longer or shorter above the ocean surface, and it will certainly depend on the relative humidity level. In order for the reflectivity to be significant in uniform, isotropic turbulence, the radar wavelength must be within the inertial subrange.

### C. Comparison of Rayleigh and Bragg Scattering

The particle distribution from Fig. 2 can be used to compare the back-scattering reflectivity from naturally occurring aerosols with that from Bragg scattering from turbulent

eddies. This is shown in Fig. 3 for  $C_n^2 = 10^{-12} \text{ m}^{-2/3}$  and various inner scale lengths. In the atmospheric surface layer,  $C_n^2$  typically varies from  $10^{-16} \text{ m}^{-2/3}$  to  $10^{-12} \text{ m}^{-2/3}$ , with the higher value corresponding approximately to the conditions responsible for the visual blurring over a hot paved surface on a clear summer day. From Figs. 2 and 3, it is evident that the large aerosol particles dominate the Rayleigh scattering calculation, and variations of the particle densities in modes 3 and 4 have a large effect on the radar reflectivity. Also evident is the exponential fall in Bragg radar reflectivity when the wavelength falls below the inertial subrange. Both the particle distribution function and the characteristics of turbulence must be known in the scattering environment in order to make reliable predictions of the expected radar return.

The strong wavelength scaling for Rayleigh scattering clearly favors shorter wavelengths and begins to dominate over Bragg scattering beginning around the millimeter-wave regime. However, the reflectivity values in Fig. 3 are averages over fairly large distances (cross section per cubic meter). Careful study of the data in Fig. 2 reveals that the number of the larger aerosols (say,  $\leq 1\mu\text{m}$ ) is very low. According to the distribution in that figure, in a cubic volume 60 cm per side, there are approximately 2400 aerosol particles with radius between 10 and 30  $\mu\text{m}$ , but only 80 with radius larger than 30  $\mu\text{m}$ . At larger distances from the sea surface, e.g. on the deck of an aircraft carrier, the number of larger aerosol particles will be reduced even further. In that case, fluctuations in the number of large aerosols within the resolution volume will cause significant fluctuations in the measured radar echo power. One representation of the contributions to the Rayleigh reflectivity from aerosols of various sizes is shown in Fig. 4, which shows the cumulative reflectivity vs. aerosol radius. So dominant is the  $R^6$  contribution of large aerosols to the reflectivity, that a fluctuation of 15% in the number density of these aerosols larger than 30  $\mu\text{m}$  leads to approximately the same fluctuation in the total reflectivity. Of course, the radar reflectivity in Eq. 7 can be also only understood in a statistical sense, i.e. as an expected value. The degradation to the SNR from fluctuations in Bragg vs. Rayleigh reflectivity is a subject deserving of considerable research activities.

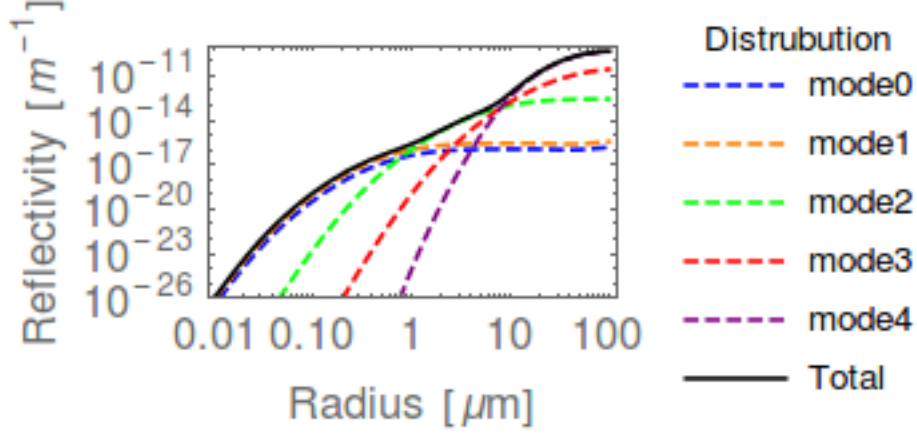


FIG. 4: The cumulative Rayleigh reflectivity vs. radius for each of the ANAM modes of the total for the atmospheric conditions of Fig. 2. The cumulative reflectivity is the reflectivity of Eq. 5 including aerosols of radius less than or equal to its argument.

#### D. Combined Bragg/Rayleigh Scattering

It is important to note that in practice aerosol particles can become trapped in the turbulent eddies. The structured aerosol density distributions produced could give rise to an enhanced back scattering that is more than the sum of Rayleigh and Bragg reflectivities. This possibility can be seen by considering the echo voltage as a composite of voltages from individual aerosol scatterers

$$V = \frac{1}{\sqrt{2}} \sum_i^{N_s} A_i W_i e^{i2kr_i}, \quad (10)$$

where  $A_i$  is the pre-filter echo amplitude,  $W_i$  is a range weighting function,  $k$  is the wavenumber, and  $r_i$  is the position of the  $i$ 'th scatterer. The echo power is then proportional to

$$|V|^2 = \frac{1}{2} \sum_i^{N_s} |A_i|^2 |W_i|^2 + \frac{1}{2} \sum_{i \neq k}^{N_s} A_i A_k^* W_i W_k^* e^{i2k(r_i - r_k)}. \quad (11)$$

The first sum represents the individual scattering contributions, and is the basis for Eq. 5. The second sum represents collective effects and typically is not considered in the literature. Entrained aerosols will impart space Fourier components on the product  $A_i W_i$ , which will lead to a Bragg type contribution to the scattering cross-section. The strengths of the collective term will depend on the amplitude and phase of the Fourier component of the  $A_i W_i$  products. Without a detailed analysis of these components, it is not possible to know

the relative values of the two sums. Some of the individual terms in the second sum will be larger in magnitude than many of the individual terms in the first sum, but the complex nature of the sum may largely wash out these contributions.

An additional consideration is that the airflow for many of the situations of interest here, e.g. that caused by and around an aircraft rotor, will be turbulent, but will be neither uniform nor isotropic. In these aero-optic regions the turbulent flow will still cascade through length scales to the inner scale length, but the spectrum of turbulent fluctuations will not follow the Kolmogorov-von Karman relation and  $C_n^2$  will vary in space. A detailed study guided by CFD simulations of the aberrating air flow is required to realistically determine the expected aero-optic effects on electromagnetic scattering. However, scattering from aero-optic turbulence can be much stronger than that from atmospheric (uniform, isotropic) turbulence, as in the former case, energy is deposited directly into higher space Fourier components.

### III. AIR FLOW MEASUREMENTS WITH RADAR

The same equation describes the total backscattered power,  $P_r$ , for lidar and radar. The Probert-Jones form of this equation for pulsed radar systems at range  $R$  is

$$P_r = P_s \left( \frac{G^2 \lambda^2 \theta \phi}{1024 (\ln 2) \pi^2} \right) \left( \frac{c\tau}{R^2} \right) \eta, \quad (12)$$

where  $P_s$  is the transmitted power,  $G$  is the antenna gain,  $\theta$  and  $\phi$  are the angular beam spreads,  $c$  is the speed of light,  $\tau$  is the pulse length, and  $\eta$  is the reflectivity. For a 1 kW radar at 100 m range, with typical values for the bracketed terms, and reflectivity values in the ranges from Fig. 3, the expected radar return power is in the range from about -70 dBm to -100 dBm. For conservative values of receiver noise figure and noise bandwidth, the thermal noise power (dominant noise source) is on the order of -70 dBm, which would appear to imply low SNR values. However, even when the signal level is weaker than the noise level, standard application of radar processing techniques such as digital pulse compression and coherent processing of multiple pulses increases the SNR by over 60 dB. Fairly standard pulse compression radars have been developed which can detect signal levels below -160 dBm, and  $C_n^2$  values below  $10^{-17} \text{ m}^{-2/3}$  [6]. The effects of standard radar signal processing on the SNR are shown in Fig. 5.

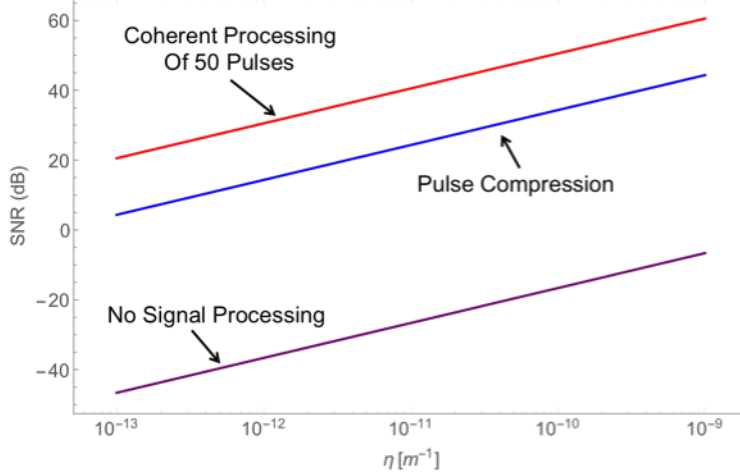


FIG. 5: Effects of standard radar signal processing techniques on the SNR of a 100 W, 94 GHz radar with 50  $\mu$ s pulses. The two-way atmospheric attenuation is approximated as 4 dB and the receiver noise figure is taken as 10 dB. The coherent processing gain curve also includes the pulse compression gain.

Photon (shot) noise overpowers thermal noise in the receiver as the wavelength decreases below 10  $\mu$ m. This was discussed in the SBIR report [1] and was shown to lead to poor SNR levels for their lidar system. There is, however, another contribution to noise that may be more important at 1.55  $\mu$ m (the lidar wavelength). This is solar spectral irradiance, which is approximately  $0.01 \text{ W cm}^{-2} \mu\text{m}^{-1}$  at the earth's surface at 1.55  $\mu$ m [7]. Assuming a receiver bandwidth of 10 MHz (to admit Doppler shifted signals of 10 m/s targets), this amounts to  $10^{-6} \text{ mW cm}^{-2}$  of background noise power density. For a  $1 \text{ cm}^2$  aperture, this is -60 dBm. Comparing this with shot noise contributions estimated at -150 dBm, and a clear air power return of -110 dBm for lidar [7] it is clear that more than 50 dB of the solar spectral irradiance must be rejected by the lidar. In contrast, a typical effective sky noise temperature for a weather radar is about 35 K, contributing only about -90 dBm of noise power in a 3 GHz bandwidth.

In the CW lidar that was developed for the Navy SBIR program, range resolution was obtained by focusing the laser beam in the range cell of interest. The radial scan rate was limited by the mechanical rate at which focusing optics could be translated. Pulsed radar systems, as well as CW radars employing specialized waveforms have a non-mechanical means for attaining range resolution. An FM chirped radar utilizes a frequency ramp in

order to obtain good range resolution and good Doppler sensitivity. The range to a target for an FM chirped radar is determined by the frequency difference between the returned pulse and a stored reference of the original pulse. The range resolution is independent of pulse length, and determined as  $\Delta R = c/2\Delta\nu$ , where  $\Delta\nu$  is the frequency bandwidth. A 300 MHz bandwidth gives a range resolution of approximately 1.5 feet. The maximum range error for a 50  $\mu$ s FM chirped pulse with a 300 MHz bandwidth is on the order of 1 inch for Doppler shifts on the order of 1-10 kHz. The corresponding velocity sensitivity is on the order of 1 m/s if the SNR is 20 dB and 0.1 m/s if the SNR increases to 40 dB.

#### IV. CONCLUSIONS

In this report, we have given preliminary considerations to the possibility of using a microwave radar to measure the air flow fields in the vicinity of naval carriers. By considering the contributions to the radar backscattering from aerosol particles, and from index of refraction variations induced by turbulent eddies, we have estimated the expected radar reflectivity values of the air flows. By considering usual performance of standard radar signal processing techniques, we have estimated the SNR that would prevail for the ranges of radar reflectivity from Bragg and Rayleigh backscattering. Our conclusions, based on these preliminary calculations are that a millimeter wave radar should be capable of producing a map of the air flow fields in the expected conditions with SNR levels above 20 dB in strong and moderate turbulence, and with sufficient levels of large water-based aerosols in the atmosphere.

- 
- [1] S. Ponniah, Technical report, Physical Optics Corporation (unpublished).
  - [2] F. Volz, *Applied Optics* **11**, 755 (1972).
  - [3] R. Doviak and Zrnić, *Doppler Radar and Weather Observations* (Academic Press, New York, 1984).
  - [4] H. Ottersten, *Radio Science* **4**, 1179 (1969).
  - [5] R. Fante, *Proc. IEEE* **63**, 1669 (1975).
  - [6] T. Ince, A. Pamany, and S. Frasier, *Geoscience and Remote Sensing Symposium I-VI*, 209 (2000).

- [7] R. Measures, *Laser Remote Sensing* (Krieger, Malabar, Fl, 1992).

